Investigation of Subsequent Viscoplastic Deformation of Austenitic Stainless Steel Subjected to Cyclic Preloading

T. Mayama[a*] Research Associate

K. Sasaki[a] Associate Professor

[a] Department of Mechanical Engineering, Hokkaido University, N13W8, Kita-ku, Sapporo, JAPAN

Abstract

This paper investigates the effects of cyclic preloading on the subsequent viscoplastic deformation. A series of experiments such as the subsequent creep, subsequent stress relaxation, and cyclic loading with strain rate changes after cyclic preloading were conducted with Type 304 stainless steel at room temperature. The cyclic proportional and non-proportional loadings were conducted as cyclic preloadings. Tension-compression loading was chosen as the cyclic proportional loading, and circular and cruciform loading as the cyclic non-proportional loading. The experimental results showed that the subsequent deformation changes with the number of cycles of cyclic preloading. The differences in the subsequent deformation were examined by transmission electron microscopy (TEM). The observations suggest that changes in the dislocation structure depending on the number of cycles of cyclic preloading affect the subsequent viscoplastic deformation.

Keywords: Creep; Dislocations; Stress relaxation; Cyclic loading; Viscoplastic material; Electron microscopy; Mechanical testing

*Tel.:+81-11-706-6416; fax:+81-11-706-6416.

E-mail address: mayama-t@eng.hokudai.ac.jp

1. Introduction

Recently, extensive research on the subsequent deformations of materials subjected to preloading has been carried out. The stress reversal Bauschinger effect, i.e. the difference in yield stress in tension and compression, is a well known subsequent deformation. This phenomenon must be considered for a precise modeling when forming sheet metals and considering subsequent springback predictions (Chun et al., 2002a, b; Yoshida et al., 2002a, b; Chung et al., 2005; Lee et al., 2005a, b). Mollica et al. (2001) developed a general three dimensional model, which can reproduce the stress-strain response at loading reversals and can be applied to more general changes in loading direction. Deformation induced anisotropy, which leads to different subsequent deformations depending on the loading direction has also been investigated (Ishikawa, 1997; Ishikawa and Sasaki, 1998; Kalidindi, 2001; Yao and Cao, 2002; Tuğcu et al., 2002; Garmestani et al., 2002; Wu, 2002; Chiang et al., 2002; Geng et al., 2002; Wu et al., 2003; Kowalczyk and Gambin, 2004; Tsakmakis, 2004; Häusler et al., 2004; Bron and Besson, 2004; Vincent et al., 2004; Cazacu and Barlet, 2004; Kuwabara et al., 2005; Wu et al., 2005; Barlet et al., 2005). Kalidindi (2001) reviewed and summarized models of anisotropic strain hardening and deformation textures in low stacking fault energy fcc metals and reported a new approach in modeling the deformation behavior of the materials. Garmestani et al. (2002) presented a crystal plasticity based modeling framework for the evolution of anisotropy in Al-Li alloys. Loadings with stain path changes are also an important issue in subsequent deformation (Hiwatashi et al., 1997; Hiwatashi et al., 1998; Kuwabara et al., 2000; Hoc and Forest, 2001; El-Danaf et al., 2001). Hiwatashi et al. (1997) developed a model based on the microstructure and simulated deformation due to the loading with a strain-path change. Hoc and Forest (2001) conducted plane strain tests followd by uniaxial tensile tests on IF-Ti steel to determine the hardening law.

To explain the macroscopic deformation mechanisms from a microscopic point of

view micro/meso scopic observations have been conducted in recent decades (Doong et al., 1990; Jiao et al., 1995; Christ et al., 1995; Feaugas, 1999; Bocher, L. et al., 2001; Gan et al., 2002; Zisman et al., 2002; El-Madhoun et al., 2003; Jia and Fernandes, 2003, Lopes et al., 2003; Haddou et al., 2004; Trivedi et al., 2004, Zuev et al., 2004). Christ et al. (1995) showed the effect of dislocation arrangements on subsequent fatigue tests. Bocher et al. (2001) showed that the over-strengthening due to non-proportional loadings is related to the development of heterogeneous substructures. Zisman et al. (2002) examined a shear microband formed in mild steel after an orthogonal strain-path change. El-Madhoun et al. (2003) concluded that the cellular dislocation structures are low energy structures and that they govern the plastic hardening behavior of commercial purity polycrystalline aluminum.

Extensive researches on the viscoplastic deformations of austenitic stainless steel have been presented (Krempl et al., 1979; Kujawski et al., 1980; Yoshida et al., 1989). However, there are few studies on the subsequent deformations after preloading and the microscopic observations.

This paper reports a series of experiments and observations of the microstructure of austenitic stainless steel (Type 304) at room temperature to determine the effects of cyclic loading with a constant strain range on the subsequent viscoplastic deformation such as the subsequent creep, subsequent stress relaxation, and cyclic loading with strain rate changes. The cyclic proportional and non-proportional loadings were conducted as cyclic preloading. The tension-compression loading was chosen as the cyclic proportional loading, and circular and cruciform loading as the cyclic non-proportional loading. The relationship between the macroscopic stress-strain response and the microscopic dislocation structure is discussed.

2. Experimental procedures

The specimens used in this study were a drawn tube of Type 304 stainless steel

subjected to solution heat treatment. The tube had a 32mm outer diameter and 6mm wall thickness and was annealed by the manufacturer at 1070℃ followed by water quenching for half an hour. The chemical compositions were 0.02C, 0.45Si, 1.09Mn, 0.030P, 0.005S, 8.30Ni, 18.54Cr, and Fe balance in weight percent. Tubular specimens were machined from this tube as shown in Fig.1. The specimens were fabricated by metal cutting and then annealed to ensure an initial isotropic stress state. In the annealing process, the specimens were heated and maintained at 380℃ for 120min followed by air cooling. Young's modulus of the specimen at room temperature was E=200GPa.

A servo-controlled axial-torsional testing machine (Shimazu EHF-EB10), with a Shimazu 4825 controller and personal computer, were used for the computerized testing and data acquisition. Strain was measured using two strain gauges applied on opposite sides of the specimen. The axial force was measured using the load cell in the machine.

Four types of tests were conducted at room temperature: (1) the tension-compression cyclic loading at strain rate 0.01%/sec with strain range 1%; (2) the subsequent creep tests after 10 and 30 cycles of tension-compression cyclic loading at strain rate 0.01%/sec with strain range 1%; (3) the subsequent stress relaxation tests at 0.5% tensile strain after 10, 30, or 100 cycles of tension-compression cyclic loading at strain rate 0.01%/sec with strain range 1%; (4) the cyclic loading with strain rate changes for measurement of the deviation of stresses between fast and slow strain rates; and (5) the subsequent creep tests after non-proportional cyclic loading at the equivalent strain rate 0.01%/sec with an equivalent strain range 0.5%. The circular loading and cruciform loading were chosen as the non-proportional loading paths.

The observations of dislocations were performed with a JEOL JEM-2000ES (200kV) TEM. Foil specimens for TEM observations were prepared by cutting thin slices from the gauge length of the specimen parallel to the stress axis. The slices were mechanically polished on both sides and jet thinned in a solution.

3. Results and discussion

3.1 Cyclic hardening and softening during cyclic tension-compression loading

Figure 2 shows the relationship between the maximum peak stress and the number of cycles during the tension-compression cyclic loading at the strain rate 0.01%/sec with the strain range 1%. It can be seen that the maximum peak stress initially increases and that it decreases after the 20^{th} cycle in this experimental condition. Cyclic hardening and softening depends on the strain range as shown in the researches (Ohno. 1982; Mizuno et al.. 2000; Kang et al.. 2003). The cyclic loading with large strain range of type 304 stainless steel shows no cyclic softening as shown in Ohno (1982). However, in the experimental condition chosen in this study, the cyclic hardening and cyclic softening processes would result in the same maximum peak stresses. For example the maximum peak stresses of the 10^{th} and 30^{th} cycles are almost the same (315MPa). Figure 3 shows a comparison of the stress-strain curves of the 10^{th} cycle with that of the 30^{th} cycle. The stress-strain curve of the 10^{th} cycle agrees well with that of the 30^{th} cycle.

3.2 Subsequent creep and stress relaxation tests after tension-compression cyclic loading

In Fig.4 the open circles and the solid line show the creep curves at the peak stress of 315MPa in tension after 10 and 30 cycles of tension-compression cyclic loading at the strain rate of 0.01%/sec with the strain range of 1%. The creep curve after 30 cycles of preloading is smaller than that after 10 cycles although the stress-strain curves of the preloading at the 10^{th} and 30^{th} cycles are the same as shown in Fig.3. This different subsequent creep curves after the preloading can not be described by classical phenomenological constitutive models. Those models predict the same subsequent deformations if the stress-strain behavior just before the subsequent loading were same. Yoshida et al. (1989) conducted the similar subsequent experiments after the cyclic preloading. However, the cyclic loadings were carried out under the stress control and

they discussed the accumulated strain during the cyclic loading and the effects on the subsequent loading. On the other hand, in our study the cyclic loadings were carried out under strain control and there is no accumulation of strain during cyclic loading.

Figure 5 shows the relationship between the relaxed stress and time caused by the stress relaxation tests at 0.5% tensile strain after tension-compression cyclic preloading at the strain rate 0.01%/sec with the strain range 1%. In Fig.5, ○, □, ×, and ● represent the subsequent stress relaxation curves after 10, 30, 60, and 100 cycles of cyclic preloading, respectively. The stress relaxation curves after 10 and 30 cycles of preloading are clearly different as is the subsequent creep deformation, i.e. , the relaxed stress decreases with increases in the number of cycles of preloadings.

3.3 Deviation of stresses between fast and slow strain rates after cyclic preloading

Figure 6 shows a schematic diagram of stress-strain curves due to cyclic tension-compression loading with strain rate changes. After 10, 30, 60, and 100 cyclic preloadings, the strain rate changed during the cyclic loading. In Fig.6, the solid lines shows the stress-strain curves at a strain rate of 0.1 and the broken line is at 0.001%/sec. Figure 7 shows the stress-strain curve of cyclic loading with variations in strain rate. It can be seen that the stress-strain curve changes abruptly just after the strain rate changes. The deviation of stresses between the strain rate 0.1 and 0.001%/sec at the 0.3% strain were measured from points A and B in Fig.7. Table 1 shows the deviations in stress after cyclic loading of 10, 30, 60, and 100 cycles. The deviation of stress decreases with the increase in the number of cycles. In most macroscopic constitutive models (e.g. Krempl, 1987; Chaboche, 1989), the stress is ordinarily divided into kinematic hardening stress (or back stress), isotropic hardening stress (or quasi-static yield stress), and time-dependent stress (or over stress). The decrease in the deviations in the stress corresponds to the decrease of the time-dependent stress. A large time-dependent stress leads to a large creep deformation and the stress relaxation is due to the process of decreases in the time-dependent stress from the macroscopic model concepts. Therefore

the experimental results in Figs.4 and 5 are also explained by the decrease in the time-dependent stress.

3.4 Subsequent creep after non-proportional cyclic loading

Subsequent creep tests after non-proportional cyclic loading were also carried out. The strain paths were circular and cruciform loadings as shown in Fig.8 (a) and (b) because it is well known that the loading can be classified into three groups due to the non-proportionality (Tanaka et al., 1985). Proportional loading, circular loading, and cruciform loading are classified different categories. In Fig.9 the open circles and open squares show the relationship between the maximum peak stresses and the number of cycles with circular and cruciform loadings. In both cases, the maximum peak stresses initially increase for several tens of cycles, and then decrease. Compared to the result of the proportional loading shown in Fig.2, the non-proportional loading shows greater cyclic hardening than the proportional loading. Moreover, the number of cycles, where cyclic softening starts, is larger than that of the proportional loading.

The peak stresses at the 25^{th} and 300^{th} cycles are almost the same with the circular loading, and the peak stresses at the 30^{th} and 300^{th} cycles are almost the same with cruciform loading. The stress trajectories at these two cycle numbers are shown in Fig.10 (a) and (b). It may be concluded that there are no differences in the trajectories of the hardening and softening processes when the peak stresses are the same.

Figure 11 shows the subsequent creep curves at the peak stress (375MPa) in tension of the 25^{th} and 300^{th} cycles after circular loading and Fig. 12 is at the peak stress (333MPa) in tension of the 30^{th} and 300^{th} cycles after cruciform loading. Different subsequent creep curves are observed for the different numbers of cyclic non-proportional preloadings as same as the proportional loading case in Fig.4. Comparing the subsequent creep strain at 1000seconds, the subsequent creep strain after the 30^{th} cycle of proportional preloading is the largest, that after the 30^{th} cycle of cruciform preloading is smaller, and that after the 25^{th} cycle of circular preloading the

smallest.

4. Microscopic observations

To establish the reasons for the changes in time-dependent deformation due to the cyclic preloading, microscopic observations were conducted by TEM. Figures 13 (a), (b), (c), and (d) show the dislocation structures of the specimens at the initially annealed state, and after 10, 30, and 100 cycles of tension-compression cyclic loadings. Initially there are few dislocations in the specimen as shown in Fig. 13 (a). After 10 and 30 cyclic preloadings, dislocation tangles become more common as shown in Fig. 13 (b) and (c). After 100 cycles, there are dislocation cell structures as shown in Fig. 13 (d). These observations suggest that the cyclic loadings resulting in the formation of dislocation cell structures. The dislocation tangles are transient features occurring between the low dislocation density of the initially annealed state and the formation of the developed cell structures.

Many models of deformation due to cyclic loadings are based on the concept that a high dislocation density leads to only hardening. According to these models, the phenomenon that the peak stress decreases with increases in dislocation density is contradictory, and the TEM observations here suggest that both the dislocation density and the dislocation structure must be considered in a constitutive model to explain cyclic hardening and cyclic softening. The observations here suggest that cyclic hardening is mainly caused by increases in the dislocation density while cyclic softening is mainly caused by the formation of dislocation structures.

Figures 14 (a), (b), (c), and (d) show the dislocation structures after 25 and 300 cycles of circular loadings and after 30 and 300 cycles of cruciform loadings, respectively. As for the tension-compression cyclic loading, cell structures are observed during cyclic softening as shown in Fig. 14 (b) and (d), while there are no apparent cell structures but tangles are observed during the cyclic hardening as shown in Fig. 14 (a)

and (c). Comparing Fig.13 with Fig.14, it may be suggested that more dislocation tangles are present with increases in non-proportionality, i.e., the highest incidence of dislocation tangles occur in the circular preloading. The cell structures during cyclic softening (Fig. 13(d), Fig. 14(b) and (d)) depend on the cyclic preloading, larger non-proportionality of the cyclic preloading leads to smaller cell structures. Overall, the size of the cell structure correlates with the subsequent time-dependent deformation.

The creep deformation occurs due to both intra-grain sliding and inter-grain dislocation slips. The TEM observations suggest that the dislocation structures affect the differences in subsequent viscoplastic deformation.

Consequently, the subsequent viscoplastic deformation depends on the dislocation structure caused by the cyclic preloading. The dislocation structure works as an obstacle to the subsequent viscoplastic deformation such as creep, stress relaxation, and cyclic loading under different strain rates. El-Danaf et al. (2001) demonstrated a similar concept termed ‘limited barriers of twinning’ for the reduced strain hardening in shear deformation.

5. Conclusions

In this study, experimental and micro-structural investigations of subsequent viscoplastic deformation after the cyclic proportional and non-proportional loading at a constant strain rate with a constant strain range were conducted using Type 304 stainless steel at room temperature. As a result the following may be concluded:

(1) The creep curves are different for different numbers of cyclic preloadings although the stress-strain curves of the cyclic preloading just before the creep are the same. The subsequent creep strain decreases with increases in the number of cycles of cyclic preloading. This phenomenon was observed with both the proportional and non-proportional loading states.

(2) The stress relaxation curves are different for different numbers of cyclic preloadings

although the stress-strain curves of the cyclic preloading just before the stress relaxation tests are the same. The relaxed stress decreases with more cycles of cyclic preloading.

(3) The deviation in stress with fast and slow strain rates at the same strain were measured in the cyclic loading tests with variations in strain rates. The deviation decreases with increases in the number of cycles of cyclic preloading.

(4) Dislocation structures are different with different numbers of cyclic preloadings though the stress-strain curves coincide. The dislocation structures affect the viscoplastic deformation such as creep, stress relaxation, and strain rate dependence of cyclic loading.

Acknowledgements

The TEM observations were conducted at the Center for Advanced Research of Energy Conversion Materials, Hokkaido University and the support for this is gratefully acknowledged.

References

Barlet, F., Aretz, H., Yoon, J. W., Karabin, M. E., Brem, J. C., Dick, R. E., 2005. Linear transformation-based anisotropic yield functions. Int. J. Plasticity 21, 1009-1039

Bocher, L., Delobelle, P., Robinet, P., Feaugas, X., 2001. Mechanical and microstructural investigations of an austenitic stainless steel under non-proportional loadings in tension-torsion-internal and external pressure. Int. J. Plasticity 17,1491-1530

Bron, F., Besson, J., 2004. A yield function for anisotropic materials Application to aluminum alloys. Int. J. Plasticity 20, 937-963

Cazacu, O., Barlet, F., 2004. A criterion for description of anisotropy and yield differential effects in pressure-insensitive metals. Int. J. Plasticity 20, 2027-2045

Chaboche, J. L., 1989. Constitutive equations for cyclic plasticity and cyclic viscoplasticity. Int. J. Plasticity 5, 247-302

Chiang, D.-Y., Su, K.-H., Liao, C.-H., 2002. A study on subsequent yield surface based on the distributed-element model. Int. J. Plasticity 18, 51-70

Christ, H.-J., Hoffmann, G., Öttinger, O., 1995. History effects in metals during constant and variable amplitude testing I: Wavy dislocation glide behaviour. Mater. Sci. and Eng. A201, 1-12

Chun, B. K., Jinn, J. T., Lee, J. K., 2002a. Modeling the Bauschinger effect for sheet metals, part I: applications. Int. J. Plasticity 18, 571-595

Chun, B. K., Kim, H. Y., Lee, J. K., 2002b. Modeling the Bauschinger effect for sheet metals, part II: applications. Int. J. Plasticity 18, 597-616

Chung, K., Lee, M., Kim, D., Kim, C., Wenner, M. L., Barlet, F., 2005. Spring-back evaluation of automotive sheets based on isotropic-kinematic hardening laws and non-quadratic anisotropic yield functions: Part I: theory and formulation. Int. J. Plasticity 21, 861-882

Doong, S. -H., Socie, D. F., Robertson, I. M., 1990. Dislocation substructures and nonproportional hardening. J. Eng. Mater. Technol. 112, 456-464

El-Danaf, E., Kalidindi, S. R., Doherty R. D., 2001. Influence of deformation path on the strain hardening behavior and microstructure evolution in low SFE FCC metals. Int. J. Plasticity 17, 1245-1265

El-Madhoun, Y., Mohamed, A., Bassim, M. N., 2003. Cyclic stress-strain response and dislocation structures in polycrystalline aluminum. Mater. Sci. and Eng. A359 220-227

Feaugas, X., 1999. On the origin of the tensile flow stress in the stainless steel AISI 316L at 300K: back stress and effective stress. Acta. Mater. 47, 3617-3632

Gan, J., Vetrano, J. S., Khaleel, M. A., 2002. Microstructure characterization of dislocation wall structure in aluminum using transmission electron microscopy. J. Eng. Mater. Technol. 124, 297-301

Garmestani, H., Kalidindi, S. R., Williams, L., Bacaltchuk, C. M., Fountain, C., Lee, E. W., Es-Said, O. S., 2002. Modeling the evolution of anisotropy in Al-Li alloys: application to Al-Li 2090-T8E41. Int. J. Plasticity 18, 1373-1393

Geng, L., Shen, Y., Wagoner, R. H., 2002. Anisotropic hardening equations derived from reverse-bend testing. Int. J. Plasticity 18, 743-767

Haddou, H., Risbet, M., Marichal, G., Feaugas, X., 2004. The effects of grain size on the cyclic deformation behaviour of polycrystalline nickel. Mater. Sci. and Eng. A379, 102-111

Hiwatashi, S., Bael, A. V., Houtte, P. V., Teodosiu, C., 1997. Modelling of plastic anisotropy based on texture and dislocation structure. Computational Materials Science 9, 274-284

Hiwatashi, S., Bael, A. V., Houtte, P. V., Teodosiu, C., 1998. Prediction of forming limit strains under strain-path changes: application of an anisotropic model based on texture and dislocation structure. Int. J. Plasticity 14, 647-669

Häusler, O., Schick, D., and Tsakmakis, Ch., 2004. Description of plastic anisotropy effects at large deformations. Part II: the case of transverse isotropy. Int. J. Plasticity 20, 199-223

Hoc, T. and Forest, S., 2001. Polycrystal modelling of IF-Ti steel under complex loading path. Int. J. Plasticity 17, 65-85

Ishikawa, H., 1997. Subsequent yield surface probed from its current center. Int. J. Plasticity 13, 533-549

Ishikawa, H., Sasaki, K., 1998. Deformation induced anisotropy and memorized back stress in constitutive model. Int. J. Plasticity 14, 627-646

Jia, W. P., Fernandes, J. V., 2003. Mechanical behaviour and the evolution of the dislocation structure of copper polycrystal deformed under fatigue-tension and tension-fatigue sequential strain paths. Mater. Sci. and Eng. A348, 133-144

Jiao, F., Osterle, W., Portella, P. D., Ziebs, J., 1995. Biaxial path-dependence of low-cycle fatigue behaviour and microstructure of alloy 800H at room temperature. Mater. Sci. and Eng. A196, 19-24

Kalidindi, S. R., 2001. Modeling anisotropic strain hardening and deformation textures in low stacking fault energy fcc metals. Int. J. Plasticity 17, 837-860

Kang, G., Ohno, N., Nebu, A., 2003. Constitutive modeling of strain range dependent cyclic hardening. Int. J. Plasticity 19, 1801-1819

Kowalczyk, K., Gambin, W., 2004. Model of plastic anisotropy evolution with texture-dependent yield surface. Int. J. Plasticity 20, 19-54

Krempl, E., 1979. An experimental study of room temperature rate- sensitivity, creep and relaxation of AISI type 304 stainless steel. J. Mech. Phys. Solids 27, 363-375

Krempl, E., 1987. Models of viscoplasticity some comments on equilibrium (back) stress and drag stress. Acta Mechanica 69, 25-42

Kujawski, D., Kallianpur, V., Krempl, E., 1980. An experimental study of uniaxial creep, cyclic creep and relaxation of AISI type 304 stainless steel at room temperature. J. Mech. Phys. Solids 28, 129-148

Kuwabara, T., Yoshida, K., Narihara, K., Takahashi, S., 2005. Anisotropic plastic deformation of extruded aluminum alloy tube under axial forces and internal pressure.

Int. J. Plasticity 21, 101-117

Kuwabara, T., Kuroda, M., Tvergaard, V., Nomura, K., 2000. Use of abrupt strain path change for determining subsequent yield surface: experimental study with metal sheets. Acta mater. 48, 2071-2079

Lee, M., Kim, D., Kim, C., Wenner, M. L., Wagoner, R. H., Chung, K., 2005a. Spring-back evaluation of automotive sheets based on isotropic-kinematic hardening laws and non-quadratic anisotropic yield functions: Part II: characterization of material properties. Int. J. Plasticity 21, 883-914

Lee, M., Kim, D., Kim, C., Wenner, M. L., Chung, K., 2005b. Spring-back evaluation of automotive sheets based on isotropic-kinematic hardening laws and non-quadratic anisotropic yield functions: Part III: applications. Int. J. Plasticity 21, 915-953

Lopes, A. B., Barlet, F., Gracio, J. J., Duarte, J. F. F., Rauch, E. F., 2003. Effect of texture and microstructure on strain hardening anisotropy for aluminum deformed in uniaxial tension and simple shear. Int. J. Plasticity 19, 1-22

Mizuno, M., Mima, Y., Abdel-Karim, M., Ohno, N., 2000. Uniaxial ratchetting of 316FR steel at room temperature – part I: experiments. J. Eng. Mater. Technol. 122, 29-34

Mollica, F., Rajagopal, K. R., Srinivasa, A. R., 2001. The inelastic behavior of metals subject to loading reversal. Int. J. Plasticity 17, 1119-1146

Ohno, N., 1982. A constitutive model of cyclic plasticity with a nonhardening strain region. J. Appl. Mech. 49, 721-727

Tanaka, E., Murakami, S., Ooka, M., 1985. Effects of strain path shapes on non-proportional cyclic plasticity. J. Mech. Phys. Solids 33, 559-575

Trivedi, P., Field, D. P., Weiland, H., 2004. Alloying effects on dislocation substructure evolution of aluminum alloys. Int. J. Plasticity 20, 459-476

Tuğcu, P., Wu, P. D., Neale, K. W., 2002. On the predictive capabilities of anisotropic yield criteria for metals undergoing shearing deformations. Int. J. Plasticity 18,

1219-1236

Tsakmakis, Ch., 2004. Description of plastic anisotropy effects at large deformations – part I: restrictions imposed by the second law and the postulate of Il'iushin. Int. J. Plasticity 20, 167-198

Vincent, L., Calloch, S., Marquis, D., 2004. A general cyclic plasticity model taking into account yield surface distortion for multiaxial ratcheting. Int. J. Plasticity 20, 1817-1850

Wu, H.-C., 2002. Anisotropic plasticity for sheet metals using the concept of combined isotropic-kinematic hardening. Int. J. Plasticity 18, 1661-1682

Wu, P. D., Jain, M., Savoie, J., MacEwen, S. R., Tuğcu, P., Neale, K. W., 2003. Evaluation of anisotropic yield functions for aluminum sheets. Int. J. Plasticity 19, 121-138

Wu, P. D., MacEwen, S. R., Lloyd, D. J., Jain, M., Tuğcu, P., Neale, K. W., 2005. On pre-straining and the evolution of material anisotropy in sheet metals. Int. J. Plasticity 21, 723-739

Yao, H., Cao, J., 2002. Prediction of forming limit curves using an anisotropic yield function with prestrain induced backstress. Int. J. Plasticity 18, 1013-1038

Yoshida, F., Kondo, J., Kikuchi, Y., 1989. Viscoplastic behavior of sus304 stainless steel under cyclic loading at room temperature. JSME international Journal 32, 136-141

Yoshida, F., Uemori, T., Fujiwara K., 2002. Elastic-plastic behavior of steel sheets under in-plane cyclic tension-compression at large strain. Int. J. Plasticity 18, 633-659

Yoshida, F., Uemori, T., A model of large-strain cyclic plasticity describing the Bauschinger effect and workhardening stagnation. Int. J. Plasticity 18, 661-686

Zisman, A., Nesterova, E., Rybin, V., Teodosiu, C., 2002. Interfacial misorientations and underlying slip activity of a shear microband in mild steel: TEM analysis and numerical simulation. Scripta Mater. 46, 729-733

Zuev, L. B., Danilov, V. I., Poletika, T. M., Barannikova, S. A., 2004. Plastic deformation localization in commercial Zr-base alloys. Int. J. Plasticity 20, 1227-1249

Captions of figures and tables

Fig.1 The geometry of specimen

Fig.2 Relationship between peak stress and number of cycles in cyclic tension-compression loading under strain rate 0.01%/sec with strain range 1.0%

Fig.3 Stress-strain curves of 10^{th} and 30^{th} cycles

Fig.4 Subsequent creep curves at the peak stress 315MPa in tension after 10 and 30 cycles of tension-compression cyclic loading

Fig.5 Subsequent stress relaxation curves at 0.5% tensile strain after 10, 30, 60, and 100 cycles of tension-compression cyclic preloading

Fig.6 Stress-strain curves of cyclic loading with variations in the strain rate

Fig.7 Stresses at strain 0.3%. A:0.1%/sec ; B:0.001%/sec

Fig.8 Loading paths of non-proportional cyclic loading tests

(a) Circular loading

(b) Cruciform loading

Fig.9 Peak stress versus number of cycles in non-proportional cyclic loading

Fig.10 Stress trajectories at two cycle numbers of non-proportional loading tests

(a) Circular loading

(b) Cruciform loading

Fig.11 Subsequent creep curves after 25 and 300 cycles of circular loading

Fig.12 Subsequent creep curves after 30 and 300 cycles of cruciform loading

Fig.13 Dislocation structures of the initially annealed and tension-compression cyclic loaded specimens

(a) As annealed specimen

(b) After 10 cycles of tension-compression loading

(c) After 30 cycles of tension-compression loading

(d) After 100 cycles of tension-compression loading

Fig.14 Dislocation structures after cyclic non-proportional loading

(a) After 25 cycles of cyclic circular loading

(b) After 300 cycles of cyclic circular loading

(c) After 30 cycles of cyclic cruciform loading

(d) After 300 cycles of cyclic cruciform loading

Table 1 Deviation in stresses with the fast and slow strain rate changes

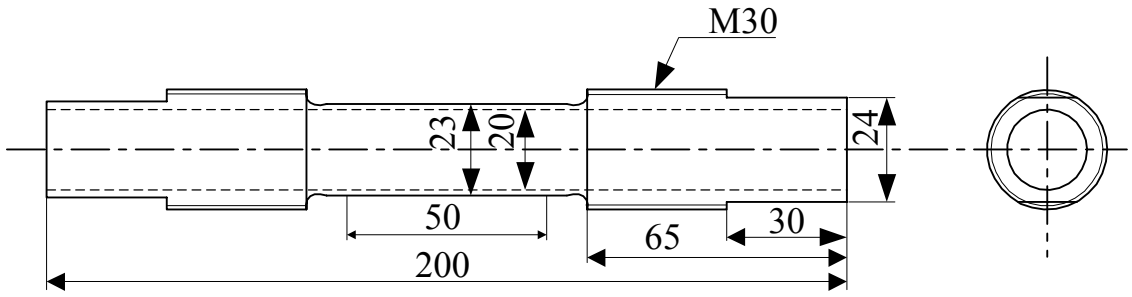

Fig.1 The geometry of specimens

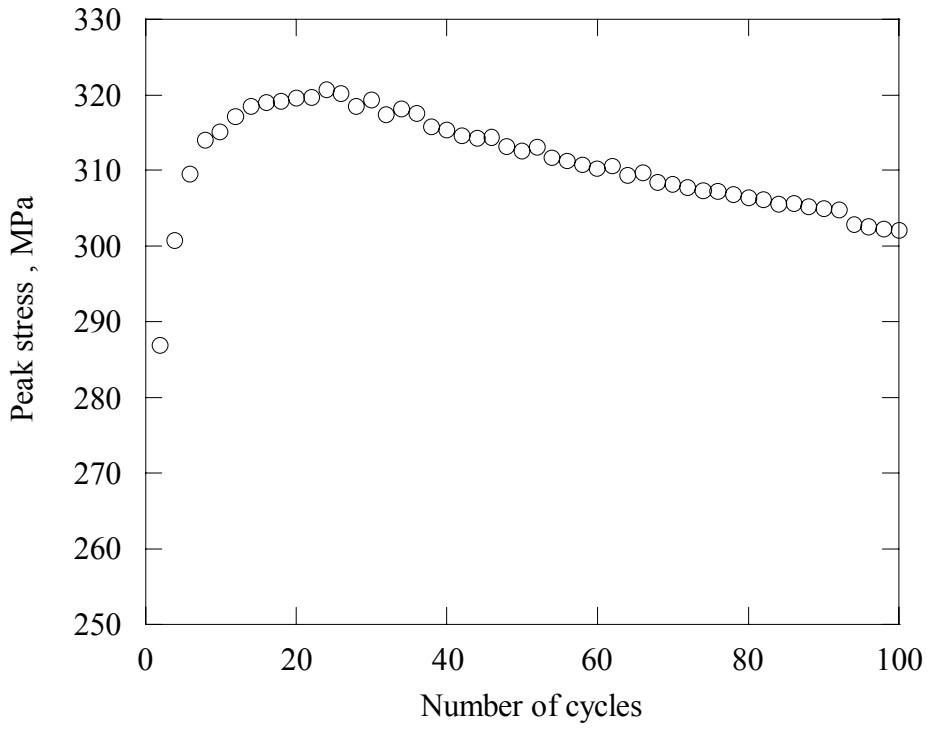

Fig.2 Relationship between peak stress and number of cycles in cyclic tension-compression loading under strain rate 0.01%/sec with strain range 1.0%

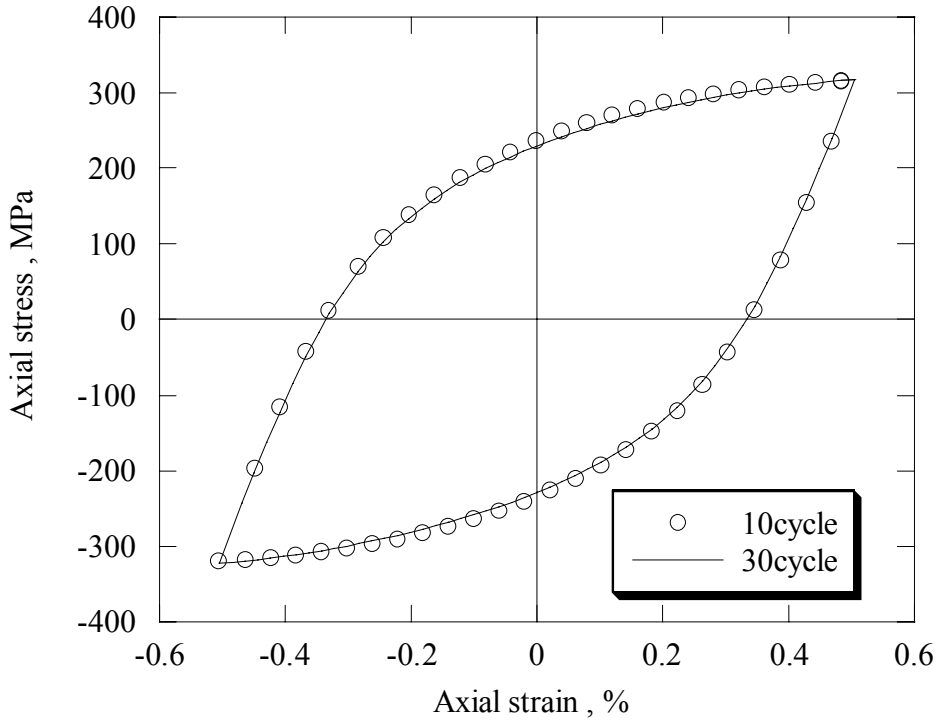

Fig.3 Stress-strain curves of 10th and 30th cycles

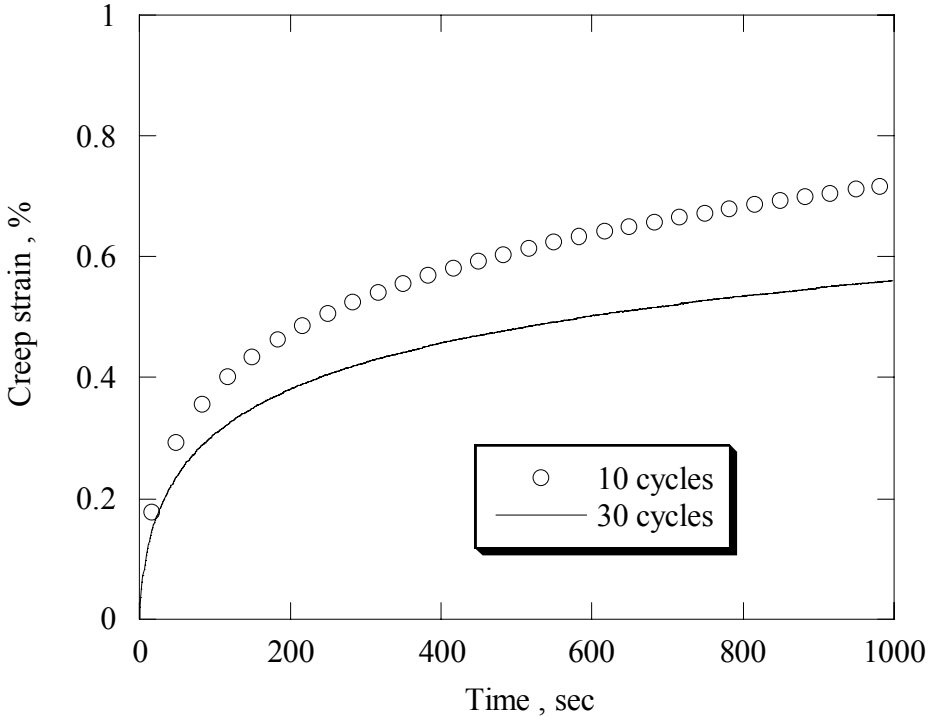

Fig.4 Subsequent creep curves at the peak stress 315MPa in tension after 10 and 30 cycles of tension-compression cyclic loading

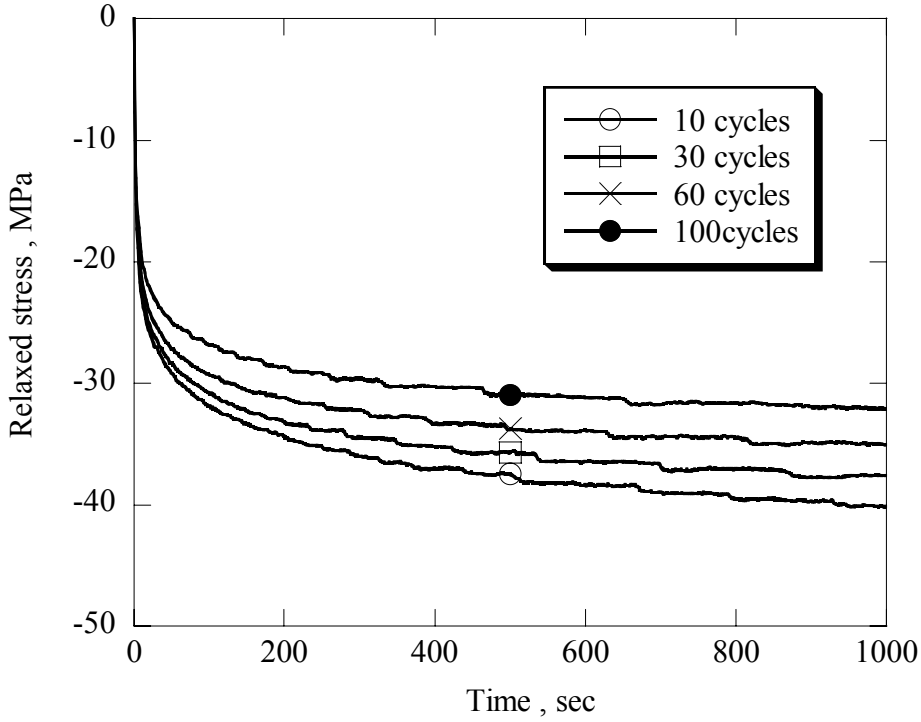

Fig.5 Subsequent stress relaxation curves at 0.5% tensile strain after 10, 30, 60, and 100 cycles of tension-compression cyclic preloading

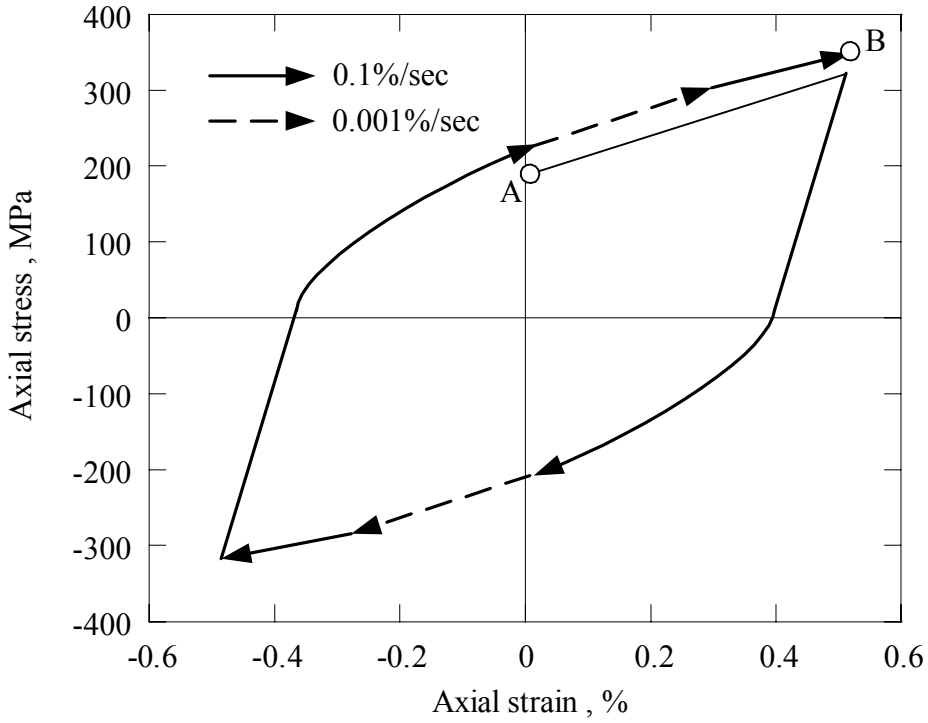

Fig.6 Stress-strain curves of cyclic loading with variations in the strain rate

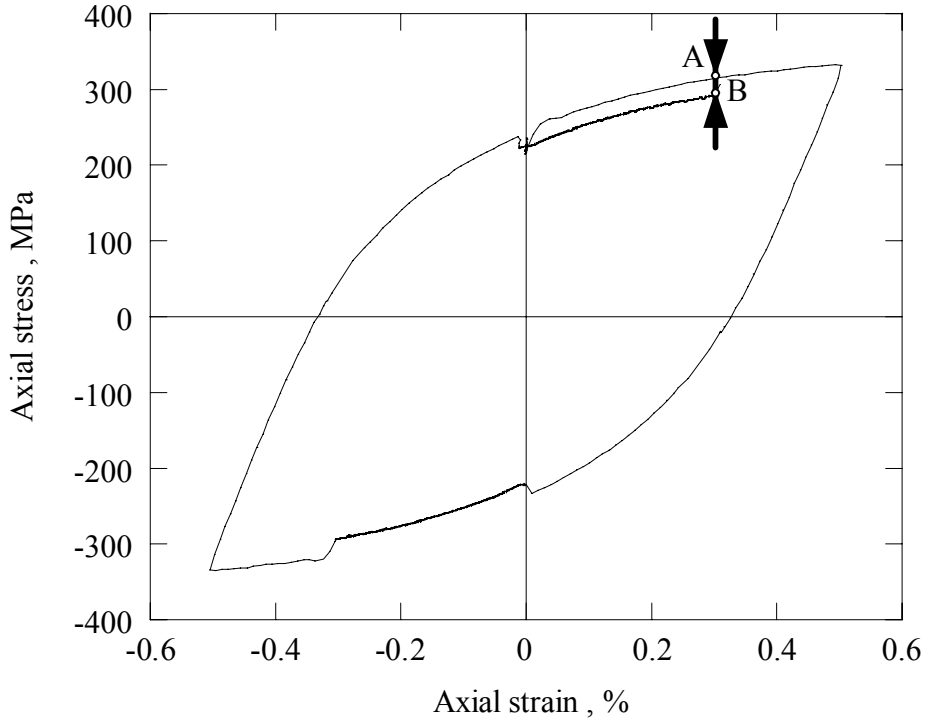

Fig.7 Stresses at strain 0.3%. A:0.1%/sec ; B:0.001%/sec

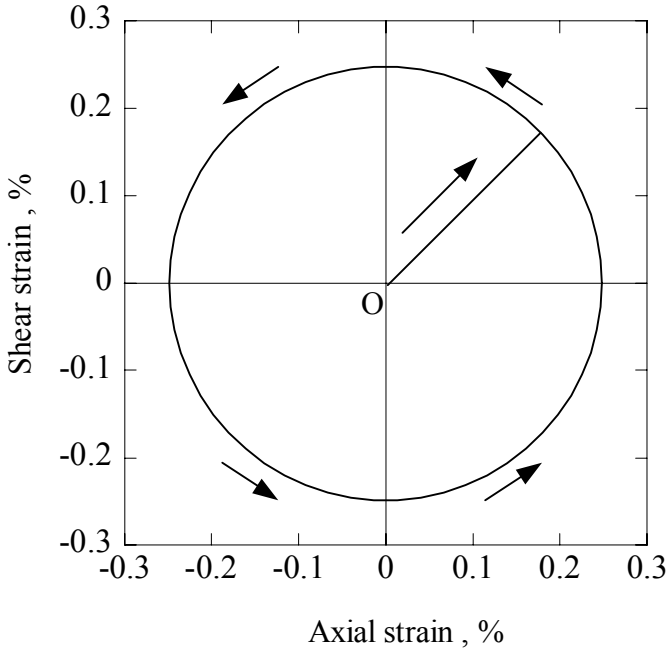

(a) Circular loading

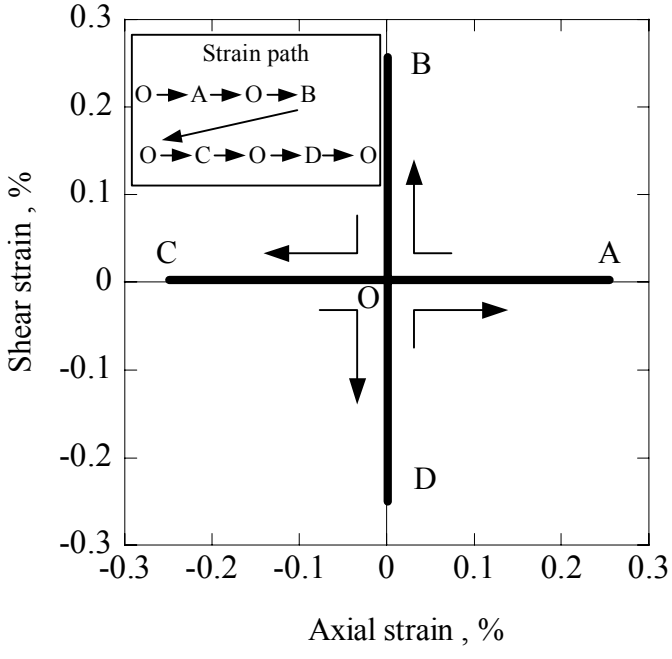

(b) Cruciform loading

Fig.8 Loading paths of non-proportional cyclic loading tests

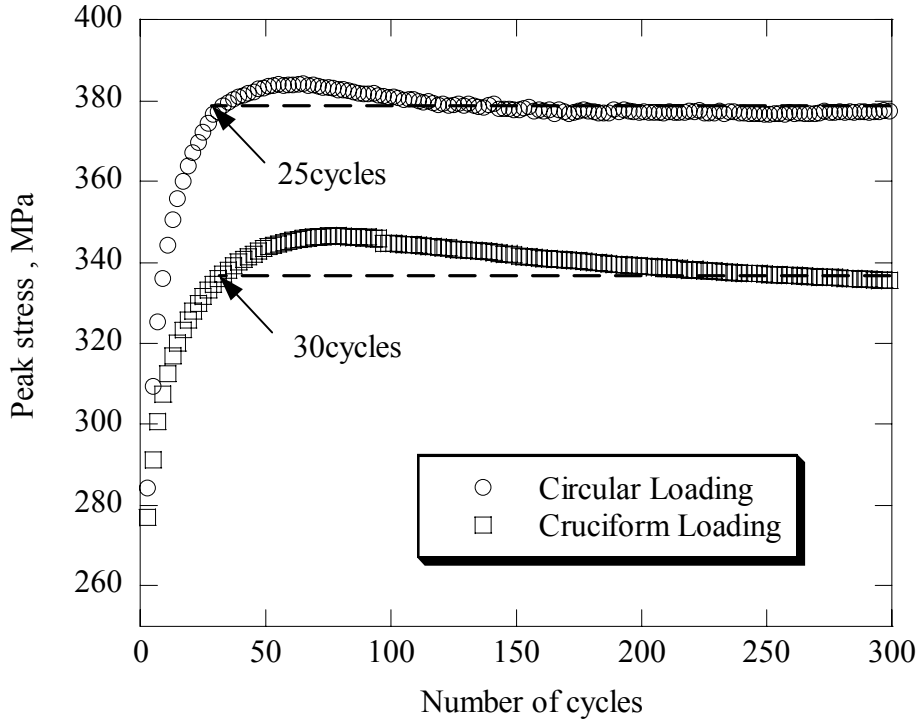

Fig.9 Peak stress versus number of cycles in non-proportional cyclic loading

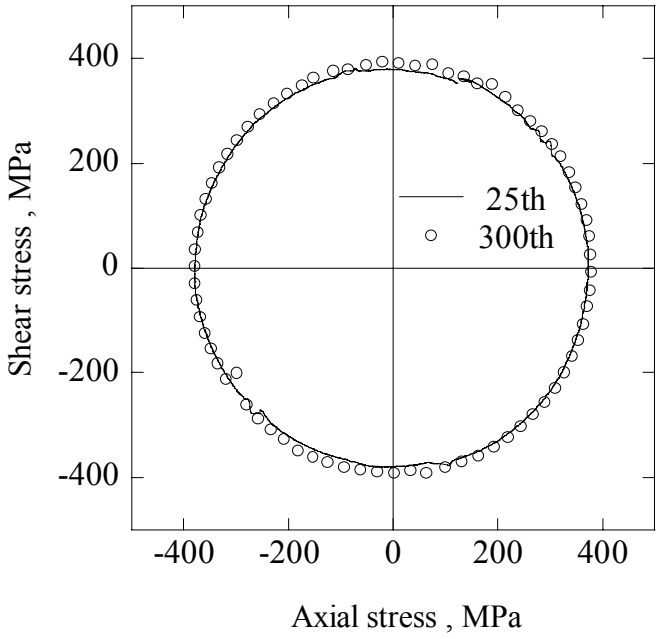

(a) Circular loading

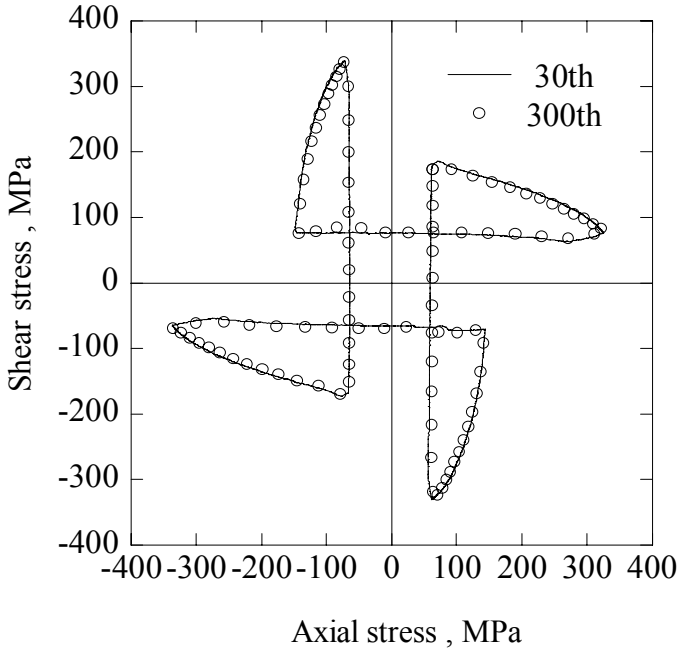

(b) Cruciform loading

Fig.10 Stress trajectories at two cycle numbers of non-proportional loading tests

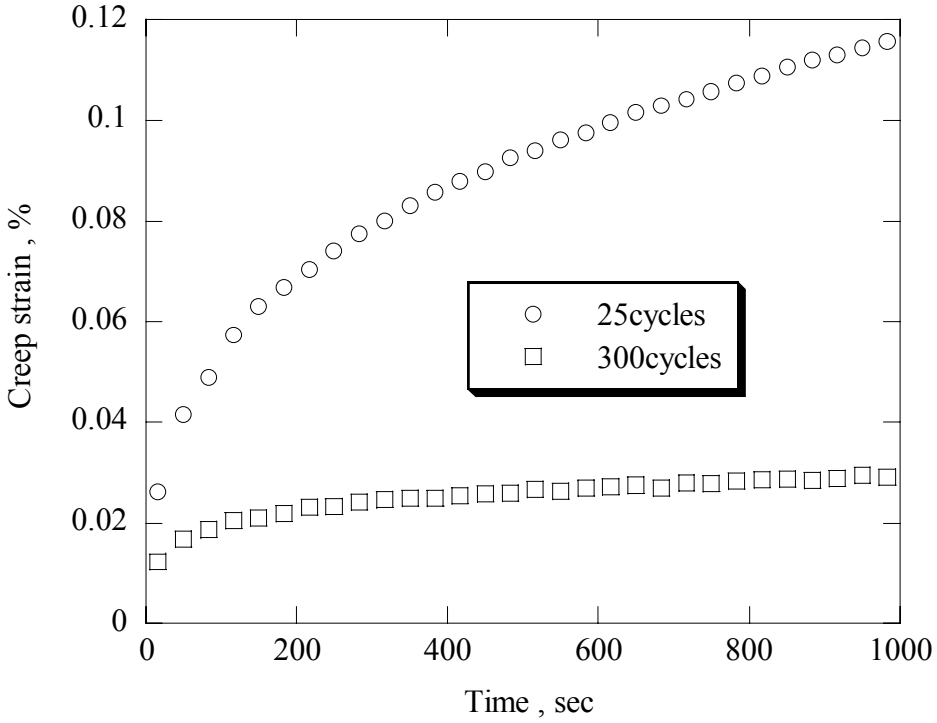

Fig.11 Subsequent creep curves after 25 and 300 cycles of circular loading

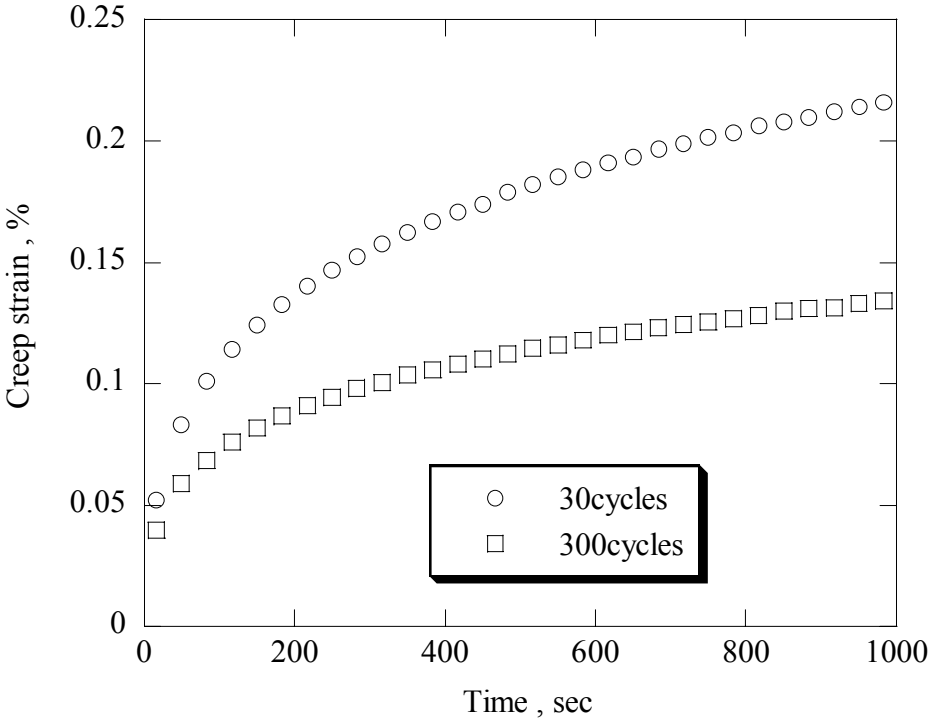

Fig.12 Subsequent creep curves after 30 and 300 cycles of cruciform loading

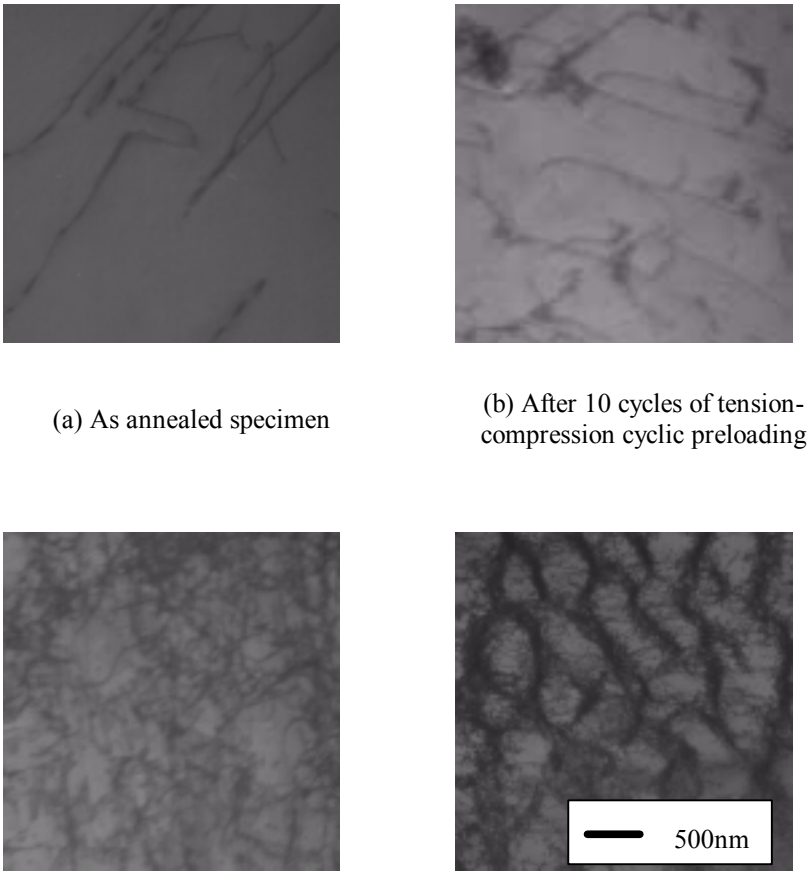

(a) As annealed specimen

(b) After 10 cycles of tension-compression cyclic preloading

(c) After 30 cycles of tension-compression cyclic preloading

(d) After 100 cycles of tension-compression cyclic preloading

Fig.13 Dislocation structures of the initially annealed and tension-compression cyclic loaded specimens

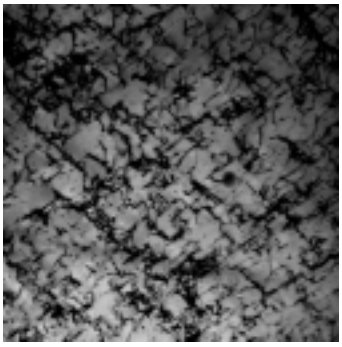

(a) After 25 cycles of cyclic circular preloading

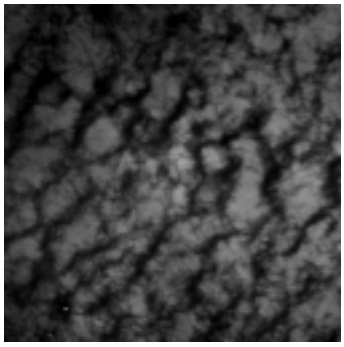

(b) After 300 cycles of cyclic circular preloading

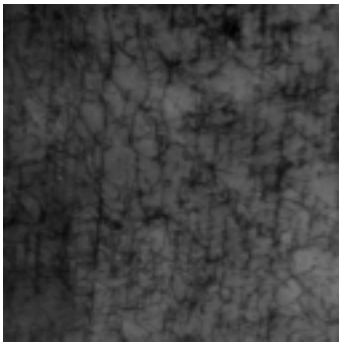

(c) After 30 cycles of cyclic cruciform preloading

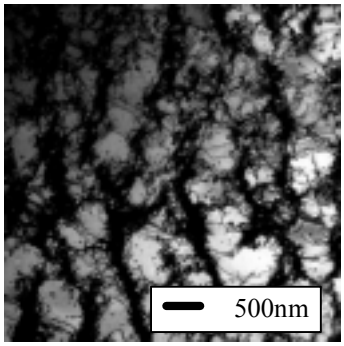

(d) After 300 cycles of cyclic cruciform preloading

Fig.14 Dislocation structures after cyclic non-proportional loading

Table 1 Deviation in stresses with the fast and slow strain rate changes

Number of cycle	10	30	60	100
Over stress [MPa]	22.9	18.5	16.9	15.2